
Laboratory Investigation to Assess the Impact of Pore Pressure Decline and Confining Stress on Shale Gas Reservoirs

KHALIL REHMAN MEMON*, ABDUL HAQUE TUNIO, AFTAB AHMED MAHESAR*,
HAFEEZ-UR-RAHMAN MEMON*, AND SHAHZAD ALI BALADI*

RECEIVED ON 10.04.2017 ACCEPTED ON 29.05.2017

ABSTRACT

Four core samples of outcrop type shale from Mancos, Marcellus, Eagle Ford, and Barnett shale formations were studied to evaluate the productivity performance and reservoir connectivity at elevated temperature and pressure. These laboratory experiments were conducted using hydrostatic permeability system with helium as test gas primarily to avoid potential significant effects of adsorption and/or associated swelling that might affect permeability.

It was found that the permeability reduction was observed due to increasing confining stress and permeability improvement was observed related to Knudsen flow and molecular slippage related to Klinkenberg effect. Through the effective permeability of rock is improved at lower pore pressures, as 1000 psi. The effective stress with relatively high flow path was identified, as 100-200 nm, in Eagle Ford core sample. However other three samples showed low marginal flow paths in low connectivity.

Key Words: Shale Gas, Effective Stress, Flow Regime, Klinkenberg.

1. INTRODUCTION

A common characteristic of all shale gas reservoirs is their extremely low intrinsic permeability. To produce gas at any significant rate, the rock must first be hydraulically fractured to create additional surface area and provide greater reservoir contact. Initially researchers [1-2] have studied the sensitivity of permeability to confining pressure at a single pore pressure. In later work intact plug permeability over a wide range of both pore and confining pressures was studied. Then researchers developed permeability-porosity relationship for mudstones using a large data set consisting of both measured permeability values

and estimates based on clay content and pore-size distribution [3-4]. A method developed for profiling permeability along a shale core sample, which was calibrated using pulse permeability measurements. As gas is produced and reservoir pressure declines, two different processes alter the permeability of the rock. These processes can be categorized as stress effects and flow regime effects. The variation of permeability with effective stress has been studied fairly extensively for sandstones and carbonates [5-7]. This is sometimes referred to as slippage flow, in reference to molecules slipping past one another. [8]

Corresponding Author (E-Mail: khalil.memon@faculty.muet.edu.pk)

*Institute of Petroleum & Natural gas Engineering Mehran University of Engineering & Technology, Jamshoro.

2. BACKGROUND STUDY ON STRESS DEPENDENT PERMEABILITY

Stress-Dependent Permeability: Many physical properties of porous rocks (permeability, volumetric strain, porosity) vary as a function of confining pressure and pore pressure according to an effective pressure. This is known as Terzaghi's principle, defined as follows:

$$\sigma_{\text{Terzaghi}} = C_p - \chi P_p \quad (1)$$

Where C_p is the confining pressure and P_p is the pore pressure. When describing how volumetric strain varies with effective stress, the appropriate coefficient is defined as the Biot coefficient, α [9-12] and effective stress law defined as confining pressure and pore pressure combination identify the permeability of the rock through effective stress law as below:

$$\sigma_{\text{eff}} = C_p - \chi P_p \quad (2)$$

Where σ_{eff} is true effective stress and χ is the effective stress coefficient for permeability. Thus, χ determines the relative sensitivity of permeability to changes in confining pressure and pore pressure. Most rocks have been shown to have $\chi \leq 1$, indicating that the rock is more sensitive to changes in confining pressure than pore pressure. However, a handful of studies of clay-bearing sandstones have found χ to be greater than 1, implying that changes in pore pressure have a larger impact on permeability than confining pressure [11-12]. In contrast to observations of $\chi > 1$ in high-clay sandstones, [13] measured $\chi \sim 1$ in very weak, high-clay Wilcox shale samples from the Gulf of Mexico. Since other studies have measured the sensitivity of gas shale matrix permeability at a single pore pressure or at a single confining pressure. However, there have been no previous studies of shale matrix permeability over a range of effective stresses and pore pressures [14-15].

3. FLOW REGIME EFFECTS ON PERMEABILITY

Expanding on the introduction above, flow in gas shale (and similarly tight rocks) is described by a combination of transport mechanisms acting at different scales [15-16]. It is common to denote transitions between these various flow regimes using the dimensionless Knudsen number, defined as:

$$Kn = \lambda d_p \quad (3)$$

Where d_p is the diameter of the pore and λ is the mean free path of a molecule moving through it, calculated as:

$$\lambda = KBoltzT \frac{zKBoltzT}{\sqrt{2}\Omega d^2 m P} \quad (4)$$

Where KBoltz is the Boltzmann constant, T is the temperature, dm is the molecular diameter, and P is the pressure. The molecular mean free path becomes larger as pressure (gas density) decreases. The relationship between the Knudsen number, pore width, and pressure is displayed in Figs. 1-2. Flow in gas shale's lies mostly within the Darcy, slip, and transition flow regimes within the petroleum engineering literature, Klinkenberg[8] was the first recognize this [8].

Fig. 1 depicts that methane at 100°C, shaded region, indicates pressure and pore size typical of gas shale reservoirs. Most of gas shale reservoirs lie within the slip and transition and Darcy flow regimes given their pore size distributions and reservoir pressure. At very small Knudsen numbers ($Kn < 0.01$), the mean free path of gas molecules is negligible relative to the pore width, and the continuum assumption (Darcy flow) is valid.

Fig. 2 shows that at the lower the pressure results in lower gas density and the larger the mean free path. The mean free path of helium is approximately double that of

methane because of its smaller molecular size. The mean free path of both increases significantly at pressures below 500 psi (3.4 MPa) approximately. Primary objective was to develop a way to estimate liquid permeability from measurements made with gas [9-15].

Theory predicts a linear trend, with y-intercept (infinite pressure) equal to the liquid permeability of the rock and the slope reflecting the changing magnitude of the mean free path with pressure relative to the effective pore width (Knudsen number) as shown in below equation.

$$k_a = k^\infty (1 + K_b/P) \quad (5)$$

Where k_a is the apparent permeability (permeability measured with gas), k^∞ is the permeability at infinite pressure (liquid permeability), K_b is the Klinkenberg parameter, and P is the mean flowing pressure across a sample. Klinkenberg cared mainly about straightforwardly obtaining liquid permeability, k^∞ , while measuring permeability with gas [9-15].

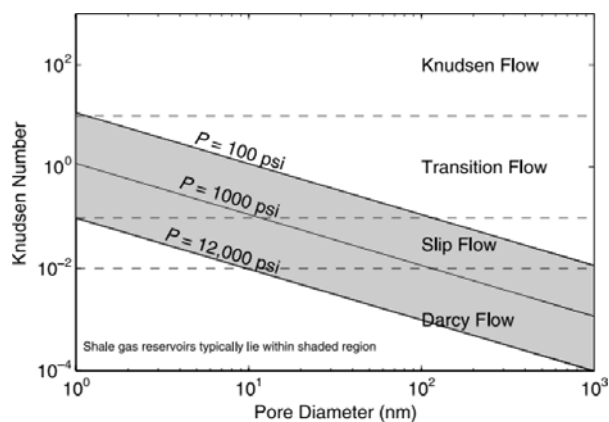


FIG. 1. DIMENSIONLESS KNUDSEN NUMBER VERSES PORE DIAMETER (NM) [8]

4. EXPERIMENTAL METHODOLOGY

All measurements were made using helium as the test gas. This was done primarily to avoid the potentially significant effects of adsorption and/or associated swelling that might impact permeability [17-19]. Sample preparation included cutting, grinding, drying, and pre-stressing. Sample plugs were initially cut to a length of approximately 3" (7.62 cm) with diameter of 1.5" (3.81cm) and size was cut down if permeability proved too low for measurements to be completed in a reasonable amount of time. The ends of each plug were ground until flat and subsequently placed in a vacuum oven at 45°C until constant mass was achieved to remove any water and/or residual hydrocarbons from the core. The temperature was chosen so as to be above the boiling point of water in near vacuum conditions, but not so high as to remove clay-bound water and alter the clay properties. Finally, the sample was loaded into the pressure vessel where it

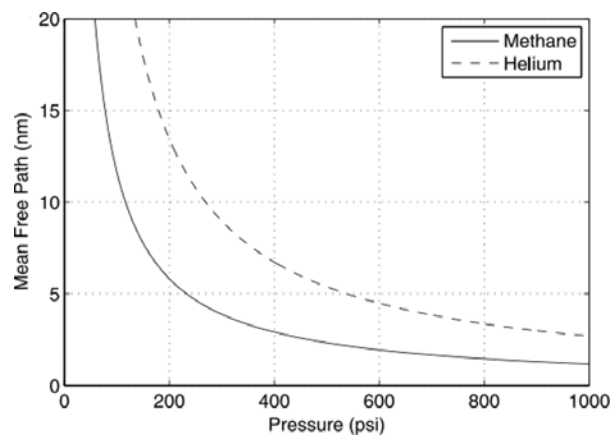


FIG. 2. FREE PATH OF METHANE AND HELIUM VERSUS PRESSURE [8]

TABLE 1. SUMMARY OF FLOW REGIMES, CORRESPONDING KNUDSEN NUMBER AND DRIVING FORCE BEHIND EACH FLUX [15]

Flow Regime	Knudsen Number	Driving Force
Knudsen/free molecule flow	$Kn > 10$	Total concentration gradient and molecular weight
Transition flow	$0.1 < Kn < 10$	Mostly Knudsen flow with some Darcy flow
Slip flow	$0.01 < Kn < 0.1$	Mostly Darcy flow with some Knudsen flow
Continuum/Darcy/Poiseuille flow	$0.01 > Kn$	Total pressure gradient

was pre-stressed for a period of 60-72 hrs at an effective stress 25% greater than the experiment design pressure. A schematic of the hydrostatic permeability system used for plug permeability measurements is shown in Fig. 2. The sample is wedged between two floating plugs attached to pore lines inside a Viton jacket. Confining pressure is controlled manually using the high-pressure generator shown on the far right in Fig. 3.

Confining pressure is measured using a Heise DXD pressure transducer accurate to 0.1% up to 10,000 psi (68.9 MPa). Pore pressure is controlled by a Quizix QX-6000 pump, equipped with two pistons capable of multiple operating modes including constant pressure, constant flow rate, and a variety of paired operating modes. The pump is capable of reaching a pressure of 6000 psi (41 MPa) as shown in Fig. 2. All flow rates were measured via the Quizix system, capable of measuring flow rates as low as 0.001 mL/min, accurate to within 0.1% of the set flow rate. Temperature within both upstream and downstream pore lines as well as the confining pressure lines is measured with thermocouples to maintain the temperature stability. Darcy flow measurements were done at approximately 1 μd for a 1.5-in. (3.81-cm) sample. The change in permeability with change in pore pressure at a given confining pressure is divided by the change in permeability with change in confining pressure at a given pore pressure. The viscous flux using the Poiseuille equation and combining this with the Knudsen flow and Klinkenberg equations as:

$$w = \frac{16cu}{K_b} \left(\frac{2RT}{\pi m} \right) \quad (6)$$

Where, w is slit width, c is an empirical constant, μ is viscosity, R is universal gas constant, T is temperature, M is molar mass, and Kb is the Klinkenberg constant.

4.1 Sample Description

In this research, A Texas Company, Kocurek Industries, Inc. provided shale core samples. Four outcrop shale types were used in the study. Mancos, Marcellus, Eagle Ford, and Barnett Shale sample. The Barnett Shale is a Mississippian-age shale located in the Forth Worth Basin in NorthCentral Texas. The Eagle Ford Shale is a Late Cretaceous-age shale located in South Texas. The Mancos Shale is an Early Triassic-age shale, located within the Western Canada Sedimentary Basin in British Columbia and Alberta. With the exception of the Marcellus plug, all samples were oriented horizontally (sample axis oriented parallel to the surface of the Earth) such that the direction of flow is parallel to the bedding. Mineralogy varies significantly from sample to sample, particularly the amount of quartz, carbonate, and clay. Both Barnett samples contained a high amount of quartz, whereas the Eagle Ford samples were dominated by carbonates and the Marcellus by clay. The Mancos sample comprised of relatively even mixture of quartz, carbonate, clay, and feldspar.

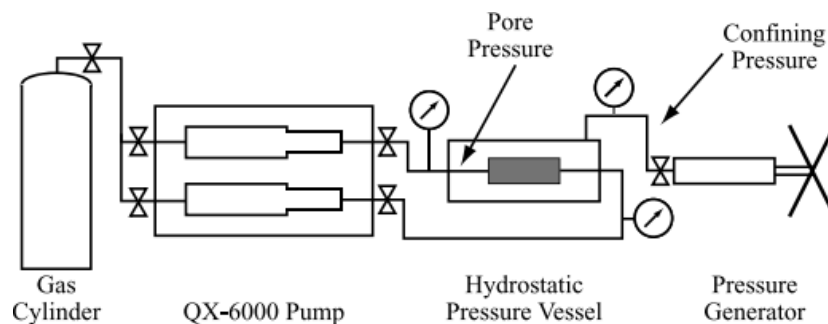


FIG. 3. HYDROSTATIC PERMEABILITY SYSTEM [17]

4.2 Results and Discussion

Plug permeability measurements were conducted for all six samples under study. Permeability was measured at pore pressures from 1000-4000 psi (6.9-27.6 MPa), confining pressures from 2000-8000 psi (13.8-55 MPa), and simple effective stresses ranging from 1000-4000 psi (6.9-27.6 MPa). These data were fit to an effective stress law. Of those six samples, three were chosen for additional permeability measurements at pore pressures below 1000 psi (6.9 MPa). The results for the high pore-pressure data (all six samples) will be presented first, followed by a more in-depth look at the rocks for which low-pressure permeability measurements were also made. Permeability as a function of simple effective stress ($C_p - P_p$) is shown for all six samples in Fig. 4. Unit of permeability in the charts on left side is in nano-Darcy and on the right side charts is micro-Darcy at different pore pressures.

Several features are worth pointing out. First, note the scale difference for the Barnett 2, Eagle Ford 2, and Mancos samples (micro-Darcy as opposed to nano-Darcy) and recall that each of these relatively high-permeability core plugs contained an anomalous carbonate layer feature. Both the Barnett 2 and Eagle Ford 2 samples contained a carbonate layer extending through the core plugs. We believe these carbonate layers are highly permeable relative to the rest of the shale matrix, resulting in a larger than typical plug permeability value in these two samples. In addition, recall that the Mancos sample contained what appeared to be a very minor crack oriented along its axis, which seems to have enhanced permeability. Finally, notice that for each sample, permeability varies as a function of simple effective stress ($C_p - P_p$) in a similar way, allowing for a single function to be fit to the whole data set. The

data for each rock were fit to a unique permeability effective stress law as described previously. These results are presented in Fig. 5.

In all cases, χ was found to be less than 1, indicating that the rocks are more sensitive to changes in confining pressure than changes in pore pressure. Noting that permeability as a function of modified effective stress forms a trend enables us to attribute all permeability variation observed (for $P_p > 1000$ psi (6.9 MPa) thus far) to effective stress effects.

As previously mentioned, three of the six samples were chosen for further characterization at lower pore pressures ($P_p < 1000$ psi (6.9 MPa)). A typical permeability sample (Eagle Ford 1), a high permeability sample (Eagle Ford 2), and a vertical sample (Marcellus) were selected for variation. Several aspects of these Klinkenberg plots are worth pointing out. First, note the increase in the Klinkenberg constant (K_b) with increasing effective stress for each rock this increase in K_b essentially represents an increase in gas slippage with increasing effective stress. This observation is intuitively reasonable, given that one would expect an increase in effective stress to narrow flow paths, thereby increasing the Knudsen number and the contribution from slip flow. It is also worthwhile to compare the magnitude of K_b between samples. Both the Eagle Ford 1 and Marcellus samples are characterized as having a similar permeability, as well as similar contributions from slip flow as evidenced by the similar K_b values.

This contrasts with the higher permeability Eagle Ford 2 sample, which has a lower K_b and, thus, a smaller overall contribution of slip flow to total flow. The overall contribution of slip flow to total flow in these samples will be further considered in the discussion section.

With Klinkenberg parameters established for each sample, we are now able to use Equation-9 to calculate the effective size of the flow paths.

Fig. 5 shows permeability versus modified effective stress after data were fit to the effect stress law for each sample. In all cases, χ was found to be less than

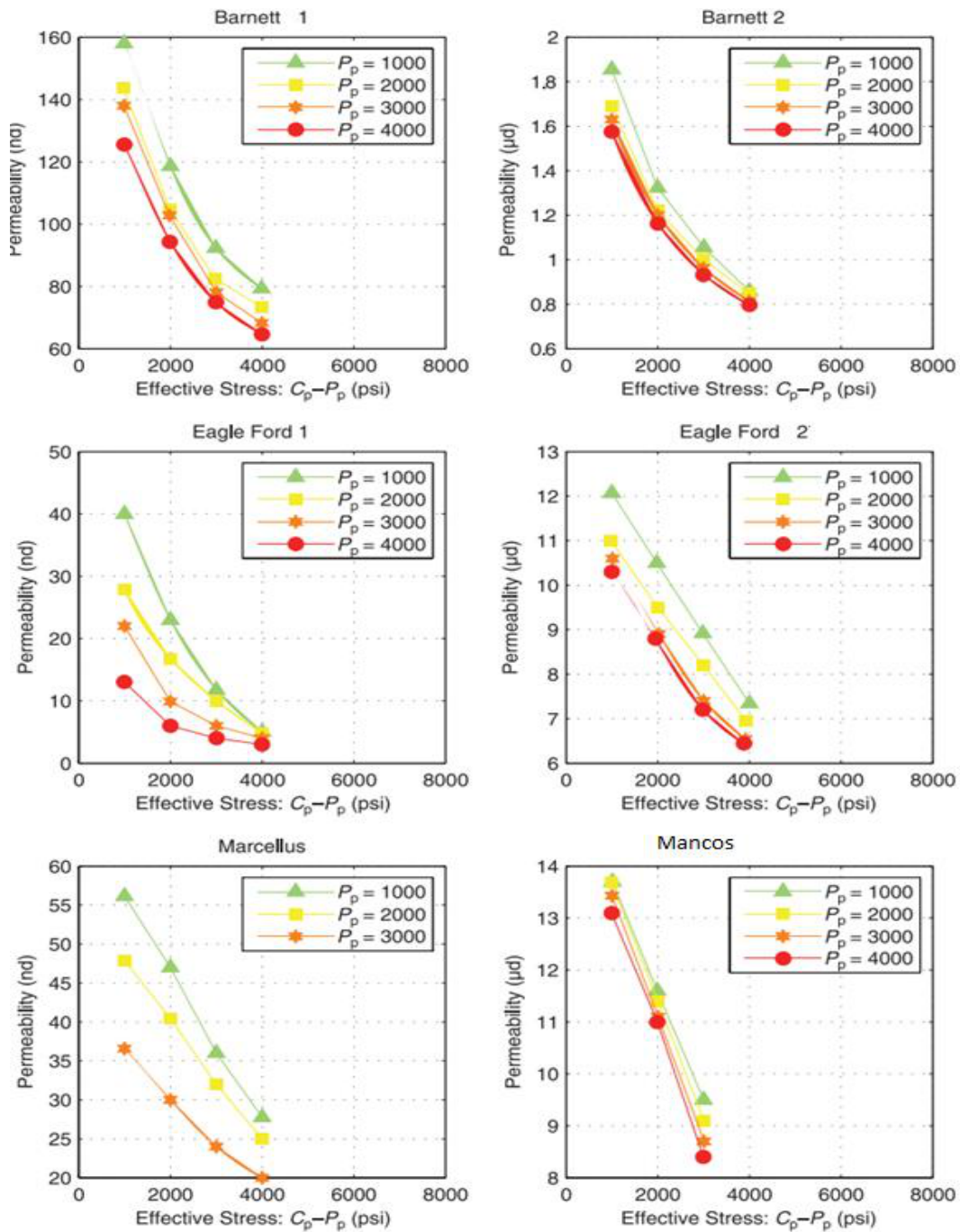


FIG. 4. PERMEABILITY VERSUS EFFECTIVE STRESS FOR ALL FOUR SHALE TYPES

1, indicating that the rocks are more sensitive to changes in confining pressure than changes in pore pressure. Noting that permeability as a function of modified effective stress forms a trend enables us to attribute all permeability variation observed (for $P_p >$

1000 psi (6.9 MPa) thus far) to effective stress effects. Because we have also determined how K_b varies with effective stress for each rock, we can estimate how the effective size of the flow paths varies with effective stress as well. Fig. 5 Left: permeability versus modified

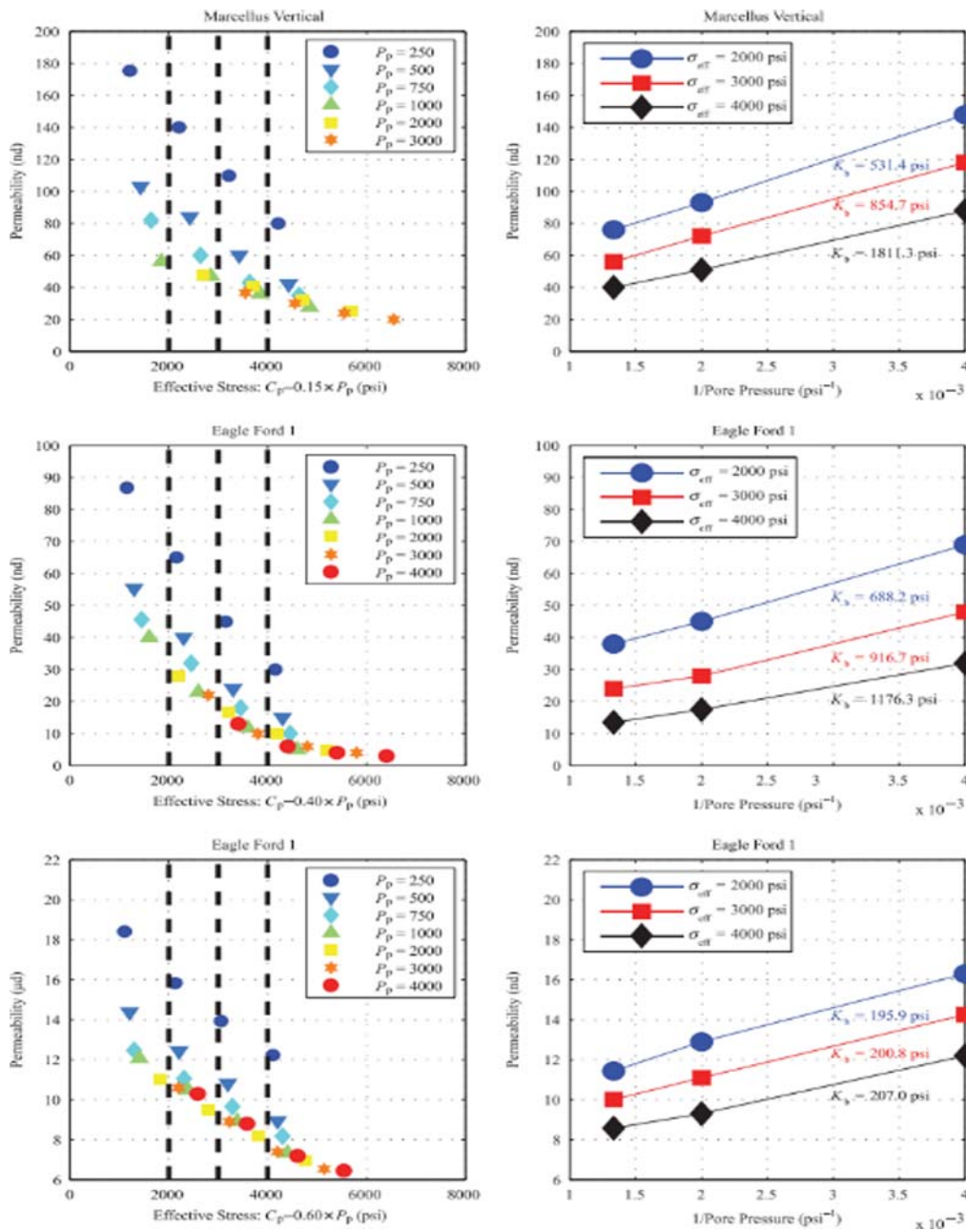


FIG. 5. PERMEABILITY VERSUS MODIFIED EFFECTIVE STRESS AT VARIOUS PORE PRESSURE

effective stress with low pore pressure data. Note the deviation from the high pore-pressure trend by the low pore pressure points. Black dashed lines indicate effective stress isolines used for generating Klinkenberg plots by selecting their intersection with the permeability trend for several pore pressures ($P_p = 250, 500, \text{ and } 750 \text{ psi}$ [$1.7, 3.4, \text{ and } 5.1 \text{ MPa}$]). Right: standard Klinkenberg plots (permeability versus $1/P_p$). Permeability points were selected for true effective stress values of $2000, 3000, \text{ and } 4000 \text{ psi}$ ($13.8, 20.7, \text{ and } 27.6 \text{ MPa}$). Notice the increase in K_b value (slope divided by intercept) with increasing effective stress.

The calculations suggest that the effective pore size varies moderately as shown in **Fig. 6**. With effective stress (about 5% in the case of Eagle Ford 2, factor of 2 in the case of Marcellus, and a factor of about 5 in the case of Eagle Ford 1). Although many assumptions went into these estimates (slit-shaped pores in particular), the results seem plausible based on the apertures of pore sizes commonly observed in SEM (Scanning Electron Microscopy).

5. CONCLUSION

A study has been conducted to impact of pore pressure decline and confining stress on shale gas reservoirs. The main conclusions in this paper are as follows:

- (i) It is observed through laboratory experiments on shale core samples examining the effects of confining stress and pore pressure of four out crop core samples were more sensitive changes in confining pressure than changes in pore pressure.
- (ii) In addition to effective stress, permeability of the rock is significantly enhanced at a very low pore pressures ($< 500 \text{ psi}$ ($< 3.4 \text{ MPa}$)) because of slippage effects.
- (iii) Increasing slip flow at low pore pressures may help to relatively long and flat production tails observed in some shale plays in Eagle Ford.

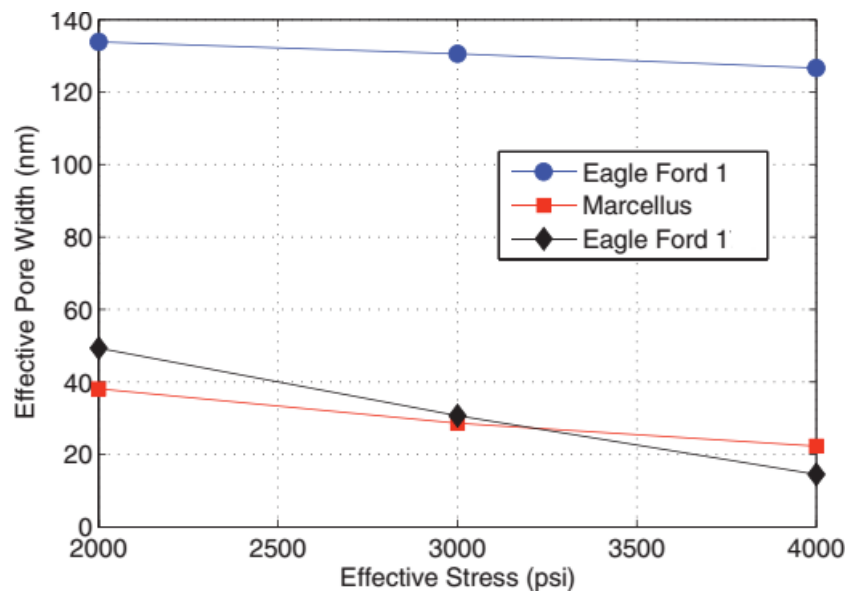


FIG. 6. EFFECTIVE PORE WIDTH VERSUS EFFECTIVE STRESS

ACKNOWLEDGEMENT

Authors wish to express my sincere thanks to, A Texas Company, Kocurek Industries, Inc. to provided shale core samples and their valuable information and furthermore my supervisors and Institute of Petroleum & Natural Gas Engineering Mehran University of Engineering & Technology, Jamshoro, Pakistan.

REFERENCES

- [1] Bustin, R.M., Bustin, A.M., Cui, A., Ross, D., and Pathi, V.M., "Impact of Shale Properties on Pore Structure and Storage Characteristics", Society of Petroleum Engineers Conference on Shale Gas Production, January, 2008.
- [2] Kang, S.M., Fathi, E., Ambrose, R.J., Akkutlu, I.Y., and Sigal, R.F., "Carbon Dioxide Storage Capacity of Organic-Rich Shales", Society of Petroleum Engineers Journal, Volume 16, No. 4, pp. 842-855, 2011.
- [3] Yang, Y., and Aplin, A.C., "A Permeability–Porosity Relationship for Mudstones", Marine and Petroleum Geology, Volume 27, No. 8, pp. 1692-1697, 2010.
- [4] Clarkson, C.R., Jensen, J.L., Pedersen, P.K., and Freeman, M., "Innovative Methods for Flow-Unit and Pore-Structure Analyses in a Tight Siltstone and Shale Gas Reservoir", AAPG Bulletin, Volume 96, No. 2, pp. 355-374, 2012.
- [5] Warpinski, N.R., and Teufel, L.W., "Determination of the Effective-Stress Law for Permeability and Deformation in Low-Permeability Rocks", Society of Petroleum Engineers Formation Evaluation, Volume 7, No. 2, pp. 123-131, 1992.
- [6] AlWardy, W., and Zimmerman, R.W., "Effective Stress Law for the Permeability of Clay Rich Sandstones", Journal of Geophysical Research: Solid Earth, Volume 109, No. B4, 2004.
- [7] Ghabezloo, S., Sulem, J., Guédon, S., and Martineau, F., "Effective Stress Law for the Permeability of a Limestone", International Journal of Rock Mechanics and Mining Sciences, Volume 46, No. 2, pp. 297-306, 2009.
- [8] Klinkenberg, L.J., "The Permeability of Porous Media to Liquids and Gases", Drilling and Production Practice, American Petroleum Institute, January, 1941.
- [9] Nur, A., and Byerlee, J., "An Exact Effective Stress Law for Elastic Deformation of Rock with Fluids", Journal of Geophysical Research, Volume 76, No. 26, pp. 6414-6419, 1971.
- [10] Zoback, M.D., and Byerlee, J.D., "Permeability and Effective Stress: Geologic Notes", AAPG Bulletin, Volume 59, No. 1, pp. 154-158, 1975.
- [11] Walls, J., and Nur, A., "Pore Pressure and Confining Pressure Dependence of Permeability in Sandstone", Transactions of 7th Formation Evaluation Symposium, pp. 1-8, October, 1979.
- [12] Kwon, O., Kronenberg, A.K., Gangi, A.F., and Johnson, B., "Permeability of Wilcox Shale and Its Effective Pressure Law", Journal of Geophysical Research: Solid Earth, Volume 106, No. B9, pp. 19339-19353, 2001.
- [13] Javadpour, F., Fisher, D., and Unsworth, M., "Nanoscale Gas Flow in Shale Gas Sediments", Journal of Canadian Petroleum Technology, Volume 46, No. 10, 2007.
- [14] Wang, F.P., and Reed, R.M., "Pore Networks and Fluid Flow in Gas Shales", Society of Petroleum Engineers Annual Technical Conference and Exhibition, January, 2009.
- [15] Schofield, R.W., Fane, A.G., and Fell, C.J.D., "Gas and Vapour Transport through Microporous Membranes", I. Knudsen-Poiseuille Transition", Journal of Membrane Science, Volume 53, No. 1-2, pp. 159-171, 1990.
- [16] Wang, F.P., and Reed, R.M., "Pore Networks and Fluid Flow in Gas Shales", Society of Petroleum Engineers Annual Technical Conference and Exhibition, January, 2009.
- [17] Cui, X., Bustin, A.M.M., and Bustin, R.M., "Measurements of Gas Permeability and Diffusivity of Tight Reservoir Rocks: Different Approaches and their Applications", Geofluids, Volume 9, No. 3, pp. 208-223, 2009.

[18] Kowalczyk, P., Furmaniak, S., Gauden, P.A., and Terzyk, A.P., "Carbon Dioxide Adsorption-Induced Deformation of Microporous Carbons", *The Journal of Physical Chemistry-C*, Volume 114, No. 11, pp. 5126-5133, 2010.

[19] Wu, K., Li, X., Wang, C., Yu, W., and Chen, Z., "Apparent Permeability for Gas Flow in Shale Reservoirs Coupling Effects of Gas Diffusion and Desorption", *Unconventional Resources Technology Conference*, 2014.